A New Method for Range Estimation Using Simple Infrared Sensors

Çağrı Yüzbaşıoğlu and Billur Barshan
Department of Electrical Engineering
Bilkent University, TR-06800 Bilkent, Ankara, Turkey
cagri@ee.bilkent.edu.tr, billur@ee.bilkent.edu.tr

Abstract— We describe a new method for position estimation of planar surfaces using simple, low-cost infrared (IR) sensors. The intensity data acquired with IR sensors depends highly on the surface properties and the configuration of the sensors with respect to the surface. Therefore, in many related studies, either the properties of the surface are determined first or certain assumptions about the surface are made to estimate the distance and the orientation of the surface relative to the sensors. We propose a novel method for position estimation of surfaces with IR sensors without the need to determine the surface properties first. The method is considered to be independent of the type of surface encountered since it is based on searching the position of the maximum value of the intensity data rather than using absolute intensity values. The method is verified experimentally with planar surfaces of different surface properties. An intelligent feature of our system is that its operating range is made adaptive based on the maximum intensity of the detected signal. The absolute mean range error for the method resulting in the lowest errors is 0.15 cm over the range from 10 to 50 cm. The cases where the azimuth and elevation angles are nonzero are considered as well. The results obtained demonstrate that IR sensors can be used for localization to an unexpectedly high accuracy without prior knowledge of the surface characteristics.

Index Terms— IR sensors, Phong illumination model, range estimation, surface localization, optical sensing

I. Introduction

An important task for many intelligent autonomous systems exploring their environment is to estimate the positions of surrounding objects as accurately as possible. Ultrasonic and IR sensors are simple, commonly employed, and relatively low-cost sensing modalities to perform this task [1]. IR sensors may be preferable to ultrasonic sensors due to their faster response time, narrower beamwidth, and lower cost. The intensity of the light detected depends on several parameters including the surface reflectance properties, the distance to the surface, and the relative orientation of the emitter, the detector, and the surface. Consequently, one problem with the use of IR sensors for position estimation is that single intensity readings are often not reliable enough to make sufficiently accurate range estimates since they are highly affected by the properties of the reflecting surface. Conversely, it is not possible to deduce the surface properties of the reflector based on a single intensity return without knowing its position and orientation, because the reflected light depends highly on the distance and the angular orientation of the reflecting surface. Due to single intensity readings not providing sufficiently accurate information about an object's position and properties, the recognition capabilities of simple IR sensors have been underestimated and underused in many applications. Although these devices are inexpensive, practical, and widely available, their use has been mostly limited to the detection of the presence or absence of objects in the environment (proximity detection) for applications such as obstacle avoidance or counting [2], [3].

One solution to the above stated problem is to employ IR sensors in conjunction with other sensing modalities to acquire information about the surface properties of the object so that the accuracy of range estimates is improved [4], [5].

A survey on the use of IR sensors can be found in [6]. In our earlier works related to IR sensing, we considered IR sensors as the only sensing modality, and used multiple intensity readings in the form of angular intensity scans for the differentiation and localization of objects [6]–[8].

In this study, we present an approach to position estimation which is relatively independent of surface type and does not require prior information about the surface. We use a pair of IR sensors, one as emitter, and the other as detector, mounted on a vertical linear platform on which they can be moved independently (Fig. 1). Both sensors make a pre-determined angle (γ) with the linear platform on which they slide. The basic idea of our method is that, while the sensors are being moved, the detector reading is maximum at some positions and the corresponding positional values of the sensors can be used for range estimation with suitable processing of the IR intensity scans. To realize this idea, for a given position of the emitter, the detector slides along the platform to collect intensity data and these data are compared to find the maximum in magnitude. The detector position corresponding to the maximum intensity data is recorded together with

Fig. 1. The experimental setup used in this study.

the corresponding *baseline separation*, which is the distance between the emitter and the detector. The distance to the surface is then estimated based on this information in a way which is relatively independent of surface type, as will be explained in more detail in Section II. In short, the system can be viewed as a variable triangulation system tuned to maximum intensity data.

Since the method is based on searching the maximum value of the intensity rather than using absolute intensity values for a given surface, it can be considered to be independent of the type of surface encountered. This is the main difference of our approach from the earlier attempts to estimate range with IR sensors. However, the type of surface inevitably affects the range of distances over which intensity data are available from a surface and determines the operating range of the system. Therefore, one can say that as long as intensity data from a surface are available, range is estimated relatively independently of the surface type.

II. POSITION ESTIMATION

The method presented in this study is based on the Phong Illumination Model [9], frequently used in computer graphics applications. This model combines the three types of reflection, which are ambient, diffuse, and specular reflection, in a single formula:

$$I = I_a k_a + I_i[k_d(\vec{l}\cdot\vec{n})] + I_i[k_s(\vec{t}\cdot\vec{v})^m] \qquad (1)$$
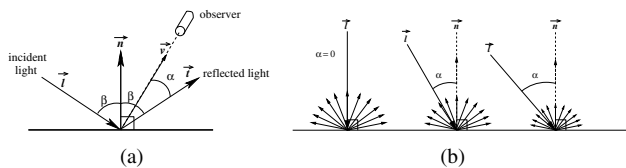

Fig. 2. (a) Specular and (b) diffuse reflection.

Here, I_a and I_i are the intensities of ambient and incident light, k_a, k_d, and k_s are the coefficients of ambient, diffuse, and specular reflections for a given material, m is the specular fall-off factor, and $\vec{l}, \vec{n}, \vec{t}, \vec{v}$ are the unit vectors representing the direction of the light source, the surface normal, the reflected light, and the viewing point, respectively (see Fig. 2(a)). In diffuse or Lambertian reflection, represented by the second term in Eqn. (1), the incident light is scattered equally in all directions and the intensity of the scattered light is proportional to the cosine of the angle between the incident light and the surface normal (Fig. 2(b)). This is known as Lambert's cosine law [10]. In specular reflection, represented by the last term in Eqn. (1), light is reflected in only one direction such that the angle of incidence equals the angle of reflection (Fig. 2(a)). In this study, the ambient reflection, the first term in the above sum, is zeroed by an IR filter, covering the detector window. Therefore, the reflected intensity is a combination of diffuse and specular components.

The position and orientation of the surface with respect to the sensors is described in spherical coordinates using r (range), θ (azimuth angle) and ϕ (elevation angle) as shown in Fig. 3. Referring to the same figure, the *sensor plane* is the plane on which the emitter, the detector, and their line of sights (LOSs) lie. The *line of interest* is the intersection of the sensor plane with the surface, which is the line from which the distance is measured or calculated. Since the linear platform stands vertically in our case, it is important to detect whether ϕ equals zero or not as the first step. The cases for $\phi = 0°$ and $\phi \neq 0°$ are investigated separately in the following two subsections.

A. Surfaces with $\phi = 0°$

When ϕ is zero, since the line of interest and the sensor platform are parallel, all maximum intensity data for different positions of the emitter should be equal to each other within some given error tolerance. Also, measured baseline separations corresponding to the maximum intensity data should be equal to each other, again within some given error tolerance. Once it is detected that $\phi = 0°$, the next step is to determine θ. In fact, the value of θ is not needed for range estimation. To show this, let us first consider the simple case where ϕ and θ are both equal to zero.

1) $\phi = 0°, \theta = 0°$: When ϕ and θ are both equal to zero, both specular and diffuse reflection components are detected. Due to specular reflection properties, the detector senses the maximum specular reflection component at position 1 where the distance a is adjusted such that the LOSs of the emitter and detector meet at the point of reflection, and consequently, $\gamma + \psi = 90°$ (Fig. 4). Here, a is half of the baseline separation between the emitter and the detector when the detector senses the maximum intensity data and γ is the acute angle between
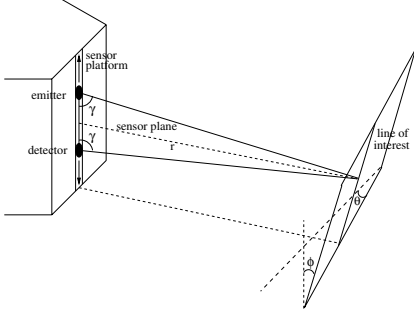
Fig. 3. The surface at (r, θ, ϕ).

(a)   (b)

Fig. 5. (a) Specular and (b) diffuse reflection when $\theta \neq 0°$.

the sensor LOS and the linear platform. Although diffusely reflected light is scattered equally in all directions as shown in Fig. 4, the detector senses the diffuse reflection component maximally again at position 1 where there is a component of the reflection in alignment with the detector LOS. Therefore, diffuse and specular reflection components act the same way to maximize the detector reading when the emitter and the detector are equidistant from the surface normal. From the geometry of Fig. 4, the distance between the sensor platform and the line of interest is given by:

$$r = a \tan \gamma \qquad (2)$$

Therefore, using the measured value of a and the known value of γ, we can estimate the range to the surface.

2) $\phi = 0°, \theta \neq 0°$: When ϕ is zero but θ is not, specular reflection does not effect the detector reading since the LOS of the detector does not lie on the plane where the specularly reflected beam propagates, as shown in Fig. 5(a). Thus, the detector reading is completely dominated by the diffuse reflection component, as illustrated in Fig. 5(b). Furthermore, only the diffusely reflected beam propagating on the sensor plane is effective whereas the others propagating on other planes are not sensed. Therefore, the situation simplifies to the representation of diffuse reflection in Fig. 4. The detector output is again maximum at position 1 where the detector LOS intersects the point of reflection so that there is a component of the diffusely reflected beam in alignment with the LOS of the detector. Hence, the distance between the linear platform and the line of interest is estimated similar to the first case, using Eqn. (2).
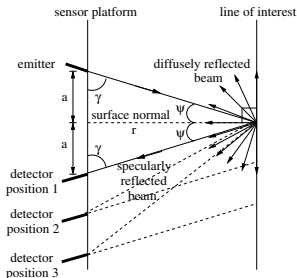

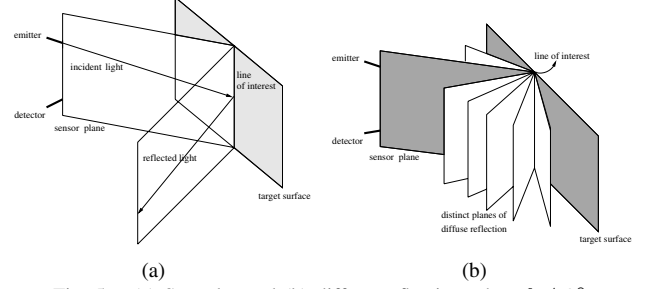Fig. 4. Sensing the specularly and diffusely reflected components.

B. Surfaces with $\phi \neq 0°$

When $\phi \neq 0°$, since the line of interest and the baseline are no longer parallel, the distance between them becomes variable. It should also be noted that similar to the $\phi = 0°$ case, the value of θ does not affect the way range is estimated. Therefore, for this case, θ is set to zero, in order not to increase the complexity of the geometry of the setup.

From the very small values of ϕ (starting at about $3°$), specular reflection becomes non-detectable by the detector since, depending on the range, the specularly reflected IR beam either reaches the detector with a large angle that remains outside the cone-like beam-pattern or is spread out of the limits of the sensor platform. As this study is realized with $5°$ increments in ϕ, the effects of specular reflection for small ϕ values ($\phi \leq 3°$) are not considered. Therefore, what the detector senses is only the diffuse reflection component.

When $\phi \neq 0°$, estimating the range by using Eqn. (2) has resulted in larger range errors than in the $\phi = 0°$ case which can be explained as follows: The rays within the cone-like beam-pattern reach the surface at different times and at different angles of incidence. The rays emitted close to the LOS of the sensor have more intensity to begin with. In addition, the rays experiencing shorter distance of travel and making smaller incidence angles with the surface normal are reflected more powerfully as described by Eqn. (1). When $\phi = 0°$, among all the rays within the cone-like beam-pattern, the ray corresponding to the brightest reflection follows the path along the LOSs of the emitter and the detector (Fig. 4). However, when $\phi \neq 0°$, the ray resulting in the highest intensity reflection is no longer the one travelling along the LOSs of the sensors. It is one of the rays either to the left or to the right of the LOS of the emitter depending on the value of ϕ. Thus, we need to add more detail to the signal reflection model, as in Fig. 6, where β is the additional angle between the LOS of the emitter and the ray resulting in the most powerful reflection. Hence, apart from ϕ, β should be determined to estimate l, which is the perpendicular distance from the most powerful reflection point to the baseline of the sensors. Note that the point where the line of length l intersects the baseline of the sensors is not the mid-point
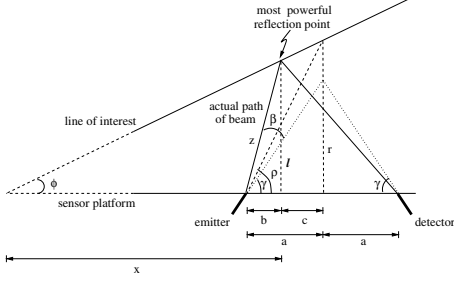
Fig. 6. The improved model of the experimental setup.

Fig. 7. Range estimation when $\phi \neq 0°$.

of the emitter-detector separation. The distance from the midpoint of the emitter-detector pair to the line of interest is r, corresponding to the actual range we want to estimate. The ρ is the angle made between the linear platform and the line connecting the emitter and the intersection point of the line segment of length r with the line of interest. As β is fixed for a specific value of ϕ, if it can be shown that ρ is also fixed, then r can be used instead of l. The details of the proof showing that ρ is fixed for a given value of ϕ can be found in [11].

The fact that ρ depends only on ϕ enables us to use ρ and r instead of $(\gamma + \beta)$ and l for range estimation. This is advantageous since the line of length r intersects the baseline at the mid-point of the emitter-detector separation, whereas the position where the line of length l intersects the baseline needs computing. The ρ values are experimentally found and recorded for different ϕ values as explained later in Section III. These will be used to find ρ values for an arbitrary value of ϕ after nonlinear curve fitting to the data.

As ρ depends on ϕ, the value of ϕ should be determined first. The procedure we used can be outlined as follows: two distinct positions of the emitter are chosen and the corresponding detector positions where maximum intensity data are observed are found as shown in Fig. 7. The distances between the emitter and the detector positions are recorded as $2a_1$ and $2a_2$, and the distance between the mid-point of the first baseline separation and the mid-point of the second baseline separation is denoted as d. From the geometry, the distance between the two emitter positions is given by $d + a_1 - a_2$, and

$$r_1 = a_1 \tan \rho \qquad (3)$$

$$r_2 = a_2 \tan \rho \qquad (4)$$

$$\tan \phi = \frac{r_2 - r_1}{d} = \frac{a_2 - a_1}{d} \tan \rho \qquad (5)$$

$$\tan \rho = \frac{d}{a_2 - a_1} \tan \phi \qquad (6)$$

where r_1 is the distance from the midpoint of emitter-detector pair to the line of interest for the first position of emitter and r_2 is the same for the second position of the emitter. Note that although we freely choose the two positions of the emitter,
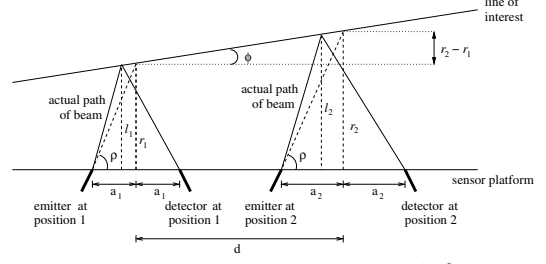
the distances a_1 and a_2, and d are determined by the positions where the maximum intensities are observed, and are, in general, dependent on ϕ. To determine this dependence, the $(a_2 - a_1)/d$ data for specific ϕ values are experimentally acquired and recorded and the corresponding $\tan \rho$ values are estimated after nonlinear curve fitting to the data. The whole procedure to estimate the range r is as follows:

- If ϕ is not zero, $(a_2 - a_1)/d$ ratio is found experimentally, and the corresponding ϕ value is read off from the line fitted to the ϕ versus $(a_2 - a_1)/d$ data (Fig. 8(b)).
- Once ϕ is estimated, $\tan \rho$ can be estimated by using the $\tan \rho$ versus ϕ curve (Fig. 8(a)).
- After $\tan \rho$ is estimated, the range to the surface is estimated using either one of Eqns. (3) or (4).

III. EXPERIMENTAL VERIFICATION

A. Experimental Setup

The experimental setup (Fig. 1) is composed of a vertical linear platform, two stepper motors, two IR sensors and a 10-bit A/D converter chip, all of which are controlled by a single PC. Both of the IR sensors [12] used in this study include an emitter and a detector in a metal casing. However, to use the sensors as a separate emitter-detector pair, the detector of one of the sensors and the emitter of the other are inhibited by covering them with an appropriately sized opaque material. The emitter and the detector both make a pre-determined angle ($\gamma = 60°$) with the platform on which they slide (Fig. 4). The sensitivity of the device can be adjusted with a potentiometer, controlled by a stepper motor, to set the operating range of the system. The detector output is interfaced to the PC after it is processed by a 10-bit A/D converter. With the present configuration, the detector output ranges between 0 to 4.9 V, where saturation occurs at 4.9 V.

The linear platform constitutes the basis for the linear motion of the detector with the help of a 5.1 W stepper motor. The step size of the stepper motor is $1.8°$ corresponding to 0.04 cm linear displacement of the detector. To be able to record the distance between the emitter and the detector, it is sufficient to keep track of the number of steps the motor takes. The second stepper motor is connected to the potentiometer of the detector to set the sensitivity of the device

automatically, as explained in more detail in Section III-B.

B. Experimental Results

The procedure we used for range estimation is as follows: For a given fixed position of the emitter, the detector starts to slide upward along the sensor platform to collect and record the intensity data and the corresponding baseline separation at each step of the stepper motor. During its motion, the detector collects 100 intensity data at each step of the stepper motor and the mean of these data is recorded together with the corresponding baseline separation. As soon as the upward motion ends, the intensity data is checked for saturation. An intelligent feature of our experimental setup is the automatic adjustment of the sensitivity of the detector to eliminate saturation. Four different sensitivity settings are available. Initially, the detector is set to the maximum sensitivity setting. If saturation is detected during the upward motion, the second stepper motor adjusts the sensitivity of the detector to a lower setting. Based on the center of gravity of the saturated intensity data acquired during the upward motion, it is possible to make a rough estimate of the distance to the surface. Using this estimate, the sensitivity of the detector can be adjusted usually in one step and the adjusted setting is used throughout the downward motion. As soon as the detector completes its motion, the intensity data are inspected to find the maximum intensity data and the corresponding baseline separation. These are recorded for the present position of the emitter. The procedure is repeated for a second position of the emitter, resulting in another set of position-intensity data.

The proposed method is verified experimentally. A planar wooden surface of dimensions 1m×0.5m×1cm is used. The surface is either left uncovered as plain wood or covered with white paper, bubbled packing material, white Styrofoam, blue, black, and red cardboard. The results are discussed in the following subsections.

1) Experimental results when $\phi = 0°, \theta = 0°$: Reference data sets are collected for each different surface, exhibiting different reflection properties, from 10 to 50 cm with 2.5 cm distance increments. As explained in Section II-A.1, for this case, it is sufficient to find the value of a. For this purpose, we used the center of gravity (COG) of the intensity curve. In this approach, a suitable threshold value is selected to retain as many samples as possible from the body of the intensity curve. Then, the COG of the intensity values remaining above the threshold is calculated as:

$$I_{COG} = \frac{\sum_{k \epsilon I_k \geq \tau} I_k a_k}{\sum_{k \epsilon I_k \geq \tau} a_k}$$

where I_k represents the intensity data sample, a_k represents half of the corresponding baseline separation, and τ is the threshold. Then, the baseline separation corresponding to I_{COG} is recorded.

	WD	WS	WP	BC	BLC	RC	LB	SB
ME	0.09	0.00	-0.15	-0.04	-0.11	-0.05	-0.11	-0.21
ABS	0.12	0.05	0.16	0.04	0.15	0.14	0.22	0.29

The experimental results are given in Table I. The overall absolute mean error in the range estimates for eight different surfaces is calculated as 0.15 cm in the range from 10 to 50 cm. The errors do not show any trend with increasing range.

2) Experimental results when $\phi = 0°, \theta \neq 0°$: When $\phi \neq 0°$, the intensity curves become significantly asymmetric (A small amount of asymmetry also exists in $\theta = 0°$ curves) [11]. Therefore, if a substantial amount of asymmetry exists, it can be concluded that $\theta \neq 0°$ as long as it is known that $\phi = 0°$. Whether $\phi = 0°$ or not is determined as discussed in Section II-B.

Measurements are collected for the wooden surface and the surface covered with white paper from 10 to 40 cm with 10 cm distance increments at values of θ ranging from $5°$ to $60°$ with $5°$ increments. The mean and absolute mean range estimation errors over 12 different θ values at each distance value are given for two surfaces in Table II. The errors start to increase for larger values of $|\theta|$ and also with increasing range. The increase of the errors with $|\theta|$ has a similar explanation as in Section II-B for the case with increasing $|\phi|$. At larger values of $|\theta|$, the effect described there is more enhanced and causes larger range errors.

In conclusion, the range is estimated in the same way regardless of whether $\theta = 0°$ or $\theta \neq 0°$. However, the value of θ affects the accuracy of range estimation since the range error increases with $|\theta|$.

3) Experimental results when $\phi \neq 0°, \theta = 0°$: In this case, reference data sets are collected for the wooden surface, for ϕ ranging from $5°$ to $45°$ with $5°$ increments. The distance between the two emitter positions $(d + a_1 - a_2)$ was chosen to be 6.3 cm. Using the reference data sets, $(a_2 - a_1)/d$ values are calculated applying the procedure explained in Section II-B and the experimental data points in Fig. 8(b) are obtained. Next, ρ values are extracted for corresponding ϕ values by measuring the actual distance r and evaluating $\tan \rho = r/a$ (Fig. 6) and Fig. 8(a) is constructed. Then, least-squares curve fitting is applied to the experimentally acquired

TABLE II

MEAN AND ABSOLUTE MEAN ERRORS WHEN $\phi = 0°$ AND $\theta \neq 0°$.

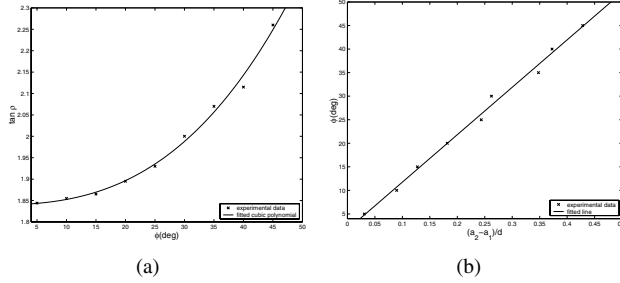|		WD				WP		
	10cm	20cm	30cm	40cm	10cm	20cm	30cm	40cm
ME	0.04	-0.58	-0.82	-0.55	-0.23	-0.72	-0.99	-0.73
ABS	0.30	0.58	0.86	0.55	0.30	0.72	0.99	0.73

Fig. 8. Experimental data for (a) $\tan\rho$ vs ϕ (b) ϕ vs $(a_2 - a_1)/d$.

ϕ versus $(a_2 - a_1)/d$ and $\tan\rho$ versus ϕ data.

Finally, a new data set is collected to be used as test data. First, the $(a_2 - a_1)/d$ value is calculated based on the two positions where the two maximum intensities are observed. The corresponding ϕ value is estimated from the fitted line shown in Fig. 8(b). Then the value of $\tan\rho$ corresponding to this estimated ϕ value is found using the fitted curve in Fig. 8(a). Finally, the range to the surface is estimated using either one of Eqns. (3) or (4). An overall absolute mean error of 0.24 cm is achieved for different ϕ and range values. This shows the effectiveness of the procedure in compensating the effects introduced by the non-zero value of ϕ.

4) Experimental results when $\phi \neq 0°, \theta \neq 0°$: Finally, to see the effects of θ when $\phi \neq 0°$, we collected reference data sets for the wooden surface for θ ranging from $5°$ to $25°$ with $5°$ increments for three values of ϕ, which are $5°$, $10°$ and $15°$. The overall absolute mean error for this case is calculated as 0.20 cm. Therefore, the overall accuracy here is of the same order of magnitude as that of $\phi \neq 0°, \theta = 0°$ case. However, remember that in the $\phi = 0°, \theta \neq 0°$ case, the error values tend to increase with increasing $|\theta|$. Therefore, it can be concluded that when both $\phi \neq 0°$ and $\theta \neq 0°$, the effects of θ being non-zero are dominated by the effects introduced by the non-zero value of ϕ. As the effects caused by non-zero ϕ value are compensated by the procedure described in Section II-B, range estimates in this case are accurate despite the effects of non-zero θ. However, the intensity plots are observed to be significantly asymmetric as in the $\phi \neq 0°, \theta = 0°$ case. Therefore, in $\phi \neq 0°$ cases, the decision of θ being zero or not needs more computing or additional data. One way to handle this situation would be to use a second detector moving perpendicularly to the first one, from which additional data regarding θ could be obtained. Such a system would be also able to detect variation in depth in both the vertical and horizontal directions

IV. CONCLUSIONS AND FUTURE WORK

In this study, a novel method for accurate range estimation of surfaces using a pair of IR sensors has been described. The method is extended to the cases where the azimuth angle θ and the elevation angle ϕ are nonzero. The absolute mean range error for the method resulting in the lowest errors is 0.15 cm over the range from 10 to 50 cm.

The experimental results obtained show that the developed system is successful in localizing planar surfaces to an unexpectedly high accuracy without prior knowledge of their surface characteristics. Instead of employing an emitter and a detector in linear motion, one can further improve the speed of the system with the use of two fixed emitters and an array of IR detectors. The system developed here is a prototype demonstrating that the method we propose indeed works and provides accurate range estimates using simple IR sensors.

The main contribution of this study is that the proposed method is relatively independent of the type of surface since it is based on searching the maximum value of the intensity rather than using absolute intensity values for a given surface which would depend on the surface properties.

Our current and future work involves improving the system performance when the azimuth angle θ is nonzero. Estimating the value of θ angle accurately will enable our system to be used in map building of unknown indoor environments. One way to increase the accuracy of angular position estimation would be to include a second detector in the system moving perpendicularly to the first one. This would provide an additional dimensionality to the present system.

REFERENCES

[1] A. M. Flynn, "Combining sonar and infrared sensors for mobile robot navigation," *Int. J. Robotics Res.*, vol. 7, pp. 5–14, Dec. 1988.
[2] E. Cheung and V. J. Lumelsky, "Proximity sensing in robot manipulator motion planning: system and implementation issues," *IEEE Trans. Robotics Autom.*, vol. 5, no:6, pp. 740–751, Dec. 1989.
[3] A. M. Sabatini, V. Genovese, E. Guglielmelli, A. Mantuano, G. Ratti, and P. Dario, "A low-cost, composite sensor array combining ultrasonic and infrared proximity sensors," *Proc. IEEE/RSJ Int. Conf. Intelli. Robots Syst.*, vol. 3, pp. 120–126, Pittsburgh, PA, 5–9 Aug. 1995.
[4] P. M. Novotny and N. J. Ferrier, "Using infrared sensors and the Phong illumination model to measure distances," *Proc. IEEE Int. Conf. Robotics Autom.*, pp. 1644–1649, Detroit, MI, 10–15 May 1999.
[5] G. Benet, F. Blanes, J. E. Simó, and P. Pérez, "Using infrared sensors for distance measurement in mobile robots," *Robotics Autonomous Syst.*, vol. 40, no:4, pp. 255–266, Sept. 2002.
[6] T. Aytaç and B. Barshan, "Simultaneous extraction of geometry and surface properties of targets using simple infrared sensors," *Opt. Eng.*, vol. 43, no:10, pp. 2437–2447, Oct. 2004.
[7] T. Aytaç and B. Barshan, "Position-invariant surface recognition and localization using infrared sensors," *Opt. Eng.*, vol. 42, no:12, pp. 3589–3594, Dec. 2003.
[8] T. Aytaç and B. Barshan, "Rule-based target differentiation and position estimation based on infrared intensity measurements," *Opt. Eng.*, vol. 42, no:6, pp. 1766–1771, June 2003.
[9] B. T. Phong, "Illumination for computer generated pictures," *Communications of the ACM*, vol.18, no:6, pp. 311–317, June 1975.
[10] M. Born and E. Wolf, *Principles of Optics*, p. 182, Oxford UK Pergamon, 6th ed., 1980.
[11] Ç. Yüzbaşıoğlu and B. Barshan, "Improved range estimation using simple infrared sensors without prior knowledge of surface characteristics," *Meas. Sci. Technol.*, vol. 16, no:7, pp. 1395–1409, July 2005.
[12] Matrix Elektronik, AG, Kirchweg 24 CH-5422 Oberehrendingen, Switzerland, *IRS-U-4A Proximity Switch Datasheet*, 1995.